Alteration of Hemodynamics in a Stented Lateral Aneurysm Model by Blocking Ratios

TONG-MIIN LIOU and YI-CHEN LI
Department of Power Mechanical Engineering
National Tsing Hua University
101, Section 2, Kuang-Fu Road, Hsinchu, Taiwan 30013.
ROC (TAIWAN)

Abstract: - This study adopts numerical simulation to discuss the fluid flow inside the stented lateral aneurysm arising from the straight parent vessel. The implicit solver was based on the time-dependent incompressible Navier-Stokes equations of laminar flow. Solutions were generated by a cell-center finite-volume method that used second order upwind and second order center flux difference splitting for the convection and diffusion term, respectively. The second order Crank-Nicolson method was used in the time integration term. To handle the pressure-velocity coupling the SIMPLEC algorithm was adopted. Complementary flow visualization was performed to validate the numerical code. The straight afferent vessel had an inner diameter 10 mm. The diameters of the aneurysmal orifice, neck, and fundus were 14 mm, 10 mm, 15 mm, respectively, and the distance between the orifice and dome measured 20 mm. A 30 mm long helix-shaped stent with four blocking ratios of 0%, 30%, 50%, 75% were examined. The density and dynamic viscosity of working fluid were 1050 kg/m^3 and 3.5 cp, respectively. Human volume flow rate waveform of the posterior carotid artery was considered with maximum Reynolds number of 250 and Wormersley number of 3.9. Computational results are presented in terms of the pulsatile main and secondary flow velocity vector fields, inflow velocity (IV) into the aneurysm, and the distributions of wall shear rate (WSR), and wall tension stress. It is found that as the blocking ratio increases, both the IV and WSR decrease exponentially. In general, the hemodynamic flow patterns and parameters examined are found to change favorably for the formation of thrombosis after stenting.

Key-Words: - Stented Lateral Aneurysms, Posterior Cerebral Artery, Blocking Ratio, Wall Shear Stress and Pressure, Flow Rate Waveform, Numerical Simulation, Laser light-sheet flow visualization

1 Introduction

Intracranial aneurysms commonly arise in the cerebral arterial circle and in most of time at the bifurcating or curved vessels. The occurrence and growth mechanism of the aneurysms are still far from clear, but according to some related studies on aneurysm pathology, factors such as inherited weakness of artery wall, hypertension, and atherosclerosis, etc., are more likely to lead to the formation of aneurysms. Furthermore hemodynamic factors, such as vessel velocity, wall shear stress and pressure all have great influences on the growth and rupture of the aneurysms [1].

As it was pointed out by Suzuki and Ohara [2], the genesis of the aneurysm is from the gap in the media, and its further growth is brought about by hemodynamic forces and blood streams, which will lead to the irregularity in the dome wall thickness with extremely thin portions and the neck wall reinforced by proliferation of intima. As a result, the dome region is considered at high risk of rupture. This finding basically correlates with the trend (Fig. 1) published by an in vivo study of Crawford [3]. In that study, among 163 ruptured aneurysms observed, rupturing in the dome region was 64% and in the fundus was 10%. Intravascular stenting [4] is thought as a better option compared with its counterpart, clipping treatment, because the use of clipping treatment cannot completely seal off an aneurysm with a wide or calcified orifice. Besides, the intravasucular stenting can be used as a complementary approach for treating saccular aneurysms with wide opening and fusiform aneurysms in which the packing agents such as balloon and/or platinum microcoils are likely to extent or migrate from the aneurysm into the parent vessel. It was also found from studies on aneruysmal treatments that stenting in the orifice could sufficiently prevent the aneurysm from rupture [4, 5].

For *in vitro* experiments on the fluid flow in the lateral aneurysms arising from a straight parent vessel, Liepsch et al. [6] discussed the differences between steady and pulsatiled flows by laser-Doppler velocimetry measurements. The influence of parent vessel curvatures on the intra-aneurysmal flow fields measured by particle tracking velocimetry (PTV) and flow visualization (FV) was reported by Liou and Liao [7], and it was found that WSS increased with

increasing curvature of the parent vessel. Liou and Liou [8] further presented the effects of stent placement on the intra-aneurysmal flow characters by PTV measurements.

For numerical studies, Burleson et al. [9] and Löw et al. [10] simulated 2-D steady and 3-D unsteady hemodynamics, respectively, in unstented sidewall aneurysms on a straight parent vessel by using the finited-element commercial code FIDAP and Galerikin finite element method together with finite differences for the time derivatives. Another study attempted to characterize the fluid flow inside the lateral aneurysms arising from the curved parent vessels at various anglesγby using both numerical and experimental studies [11]. For the stented cases, the flow through stented aneurysms was analyzed by the use of 2-D finite element method in the study of Stuhne and Steinman [12]; the fluid flow of aneurysms on the straight parent vessel with trio stent has also been presented by the use of 3-D finite element [13]; the same method has also been adopted by Stuhne and Steinman [12] in their investigation on 4-layer helix stented flow field of aneurysm on a straight parent vessel.

To conclude what has been discussed above, it is found that stending can efficiently treat the aneurysms. But no study has been carried out to discuss the impace of different blocking ratios of the same stent shape on the aneurysmal hemodynamic characteristics. Furthermore because of the insufficiency in the experimental techniques and the difficulties in collecting information on hemodynamic factors, this study adopts both numerical simulation and experiment. In the following discussion, both experimental verification of the numerical simulation and the numerical evaluation on the influences of different blocking fations on the hemodynamic factors in the aneurysm which arises from the posterior carotid artery (PCA) will be presented.

2. Theoretic formulation and numerical solution

2.1 Geometry and coordinate system of calculation domain

Figure 1 shows the configuration, coordinate system, dimensions, and grid distribution of the main computational domain. The coordinate origin was chosen at the center of aneurysmal pore with the X-axis along the tangential direction of parent vessel and Z-axis directed to the dome along the aneurysmal centerline. The blocking ratios, C_α=Nd/L, of the 30 mm (L) long stents with a helix shape were 0% (stentless), 30%, 50% and 75%. N and d are the number of pitches and the diameter of the stent filament, respectively. There existed 60D long straight vessel sections upstream and downstream of main computational domain for attaining the fully developed state.

2.2 Governing equations and boundary conditions

Since in larger vessels (D>0.5mm), such as aorta and major arteries, blood behaves more or less as a Newtonian fluid [14], an incompressible Newtonian fluid is considered for the PCA examined (D=2.0±0.5mm [15]). The fluid is assumed to be homogeneous and isothermal with negligible gravity effects. Thus, the governing equations take the following dimensionless form:

(a) continuity equation

$$\nabla \bullet \vec{U} = 0 \qquad (1)$$

(b) momentum equations

$$\frac{1}{\pi}\frac{\alpha^2}{\mathrm{Re_M}}\frac{\partial \vec{U}}{\partial t} + (\vec{U}\bullet\nabla)\vec{U} = -\nabla P + \frac{2}{\mathrm{Re_M}}\nabla^2\vec{U} \qquad (2)$$

where $\vec{U}$ denotes the dimensionless velocity vector, P the dimensionless relative pressure, $\mathrm{Re_M}=(\rho U_{max} D/\mu)=250$ [16] the maximal Reynolds number (Fig.2), $\alpha=D/2\sqrt{\rho\omega/\mu}=3.9$ [16]the Womersley number, and t the time. ρ is the density, μthe dynamic viscosity, and $\omega=2\pi/T$ the angular frequency of the oscillation. The non-dimensional WSS is $\tau_w/\rho U_{max}^2$, where τ_w (dyne/cm^2) can be written as

$$\tau_{w,ij} = \mu\left(\frac{\partial u_i}{\partial x_j} + \frac{\partial u_j}{\partial x_i}\right), (i, j = x, y, z) \qquad (3)$$

The characteristic quantities needed for defining the above dimensionless variables of u_i, p, x_i and t are the inlet maximal velocity U_{max}=8.33 cm/s of parent vessel, ρU_{max}^2, radius D/2=5mm of parent vessel, and pulsation period T=3.097s [16], respectively.

The one-period u_{in}/U_{max} waveform is shown in Fig.2. u_{in}/U_{max} is the pulsatile velocity averaged over the cross-section of the inlet reference station (volume flow rate/cross -sectional area) and is specified at 60D upstream of the aneurysmal orifice of the parent PCA (Fig.2). For the outlet boundary conditions at 60D downstream of the aneurysm orifice portion of parent vessel, zero reference pressure is assumed. At the solid wall no slip and zero normal pressure gradient conditions are used.

2.3 Numerical algorithm

Solutions were generated by an in-house cell-center finite-volume based CFD code that used second order upwind and second order center flux difference splitting for the convection and diffusion term, respectively. The second order Crank-Nicolson implicit method was used in the time integration term. To handle the pressure-velocity coupling, the SIMPLEC algorithm [17] was adopted.

This study adopts unstructured grid layout (hexahedral and tetrahedral grid). The total number of cells for the computational domain is 900,000 after grid independent test. The convergence criteria in the cell and the time step independence test of the present implicit algorithm were documented in details in our previous study on unstented lateral aneurysms arising at various angles from the internal carotid artery [11]. The time step size determined is T/100=0.3097s. For the present case with α=3.9 and the relative pulsatile flow field error smaller than 10^{-3}, three pulsatile cycles or 300 time steps were necessary in order to achieve time-periodic convergence.

3. Results and Discussion

3.1 Comparisons between numerical and experimental results

For the unstented case, at peak phase of a sinusoidal waveform the inflow in Y*= 0 plane enters the aneurysm at the downstream lip of the pore, and subsequently creates two opposite vortexes in the aneurysm sac, one prevailing in the upper half and the other prevailing in the lower half of the aneurysm. The outflow exits the aneurysm at the proximal side of the pore. After stenting the numerically computed and laser light-sheet visualized intra-aneurysmal main flow patterns are depicted in Fig.3 for C_α=50%. Reasonable agreement between the CFD and experimental results are attained. Markedly differences in the main flow patterns between the unstented and stented cases are revealed: the inflow and outflow locations are opposite and the intra-aneurysmal vertical structures are changed after stenting. The importance of the value of C_α in affecting the intra-aneurysmal main flow pattern is thus demonstrated.

The verified in-house numerical code can thus be used to explore the effects of blocking ratio on the intra-aneurysmal flow characteristics under the human cardiac waveform in the following text.

3.2 Effects of C_α on the Main Flow Pattern in Y*=0 Plane

Figure 4 displays the instantaneous intra- aneurysmal flow fields at some selected flow rate phases in Y*=0 plane with and without stent. It is seen that in general the number and size of structured vortices are reduced after stenting. In addition, when t/T=0 and t/T=0.27 to 044 (Figs. 3 and 4), the inflow into the aneurysm is shifted from the distal lip of the orifice for the unstented case to the proximal lip for the stented case. The flow reversal adjacent to the bottom wall of the parent vessel is also reduced after stenting when t/T=0.63. From Fig.4 the quantitative differences in hemodynamic factors between the unstented and stented cases can be analyzed and will be presented in the succeeding section.

3.3 Effects of C_α on Secondary Flow Pattern in X*=0 Plane

The cross-sectional secondary flow fields in X*=0 Plane of the unstented and stented cases are depicted in Fig.5 for t/T=0.27. When the parent vessel is straight, the secondary flow velocity is fairly small, less than 0.1 U_{max} even for the stentless case. For the unstented case (C_α=0%), a pair of symmetric secondary flow vortexes (Dean vortices) is present aound the upper rim of the aneurysmal lip (Z*=0.32). From this pair of vortexes it is found that the fluid leaves the aneurysm from both sides of the wall of the aneurysmal lip. The direction of the vortex pair is opposite after stenting, i.e. the fluid goes back to the parent vessel from the center of the aneurysm. With the increasing blocking ratios, the secondary velocity decelerates remarkably and the secondary vortices are gradually confined to the parent vessel.

To conclude the findings for the main and the secondary flow fields discussed in the previous sections, it is obvious that stenting can effectively reduce the main and secondary flow field structures so as to decrease the velocities at different directions in the aneurysm, and the higher the blocking ratios are, the lower the velocities in the aneurysm. Lowering the velocities in the aneurysm can promote the occurrence of the hemostasis, leading to the rapid growth of the thrombus in the aneurysm [18] so as to attain an effective treatment for the aneurysm.

3.4 Effects of C_α on Inflow Velocity into Aneurysm

From Fig.6 one sees that when C_α is 30%, the average Inflow Velocity (IV) over a cardiac cycle at the stented aneurysmal neck and fundus are 51.3% and 81.7% lower, respectively, than those for unstented case. However when comparing the average IV at the neck and the fundus when C_α are 75% and 50% for the stented case, the values for 75% are only 1.7% and 6.3% lower than those values for 50%. To sum up, the average IV at both the neck and fundus over one

cardiac cycle decrease following the $e^{-0.022C_\alpha}$ and $e^{-0.048C_\alpha}$ distributions, respectively, with the increasing blocking ratios.

The phenomenon of the decreasing inflow velocities shows the decreasing flow activity in the aneurysm, which is indicative of a higher occurrence of hemostasis. Under this circumstance, the formation of the thrombosis is easier, leading to the occlusion of the aneurysm (Tominaga et al. 1993), and resulting in an effective treatment of the aneurysm.

3.5 Wall Shear Rate and Wall tension stress

The intra-aneurysmal wall shear rate (WSR) distributions are found to change markedly from the lip of the orifice to the neck but become relative uniform from the neck to the dome. Comparing with the unstented case, one finds that the WSR at the the aneurysmal dome in different stented cases are reduced to 23.1%(C_α=30%), 9.62%(C_α=50%) and 1.9%(C_α=75%) at peak phase, respectively. Furthermore, the WSR at the dome region decreases with the increasing blocking ratios following the $e^{-0.05C_\alpha}$ distribution (Fig. 7). Therefore the placement of stent will promote the occurrence of the thrombosis and, in turn, avert the growth of aneurysm [19, 20].

The aneurysmal walls are stressed by the transmural fluid pressure in the lumen that acts to distend them. Laplace's law relates the wall pressure to the circumferentially directed average wall tension stress (WTS). Compared with the unstented case, it is found that the mean wall tension stress, averaged over a cardiac cycle, decreases with increasing blocking ratios. However the extend of the decreasing is limited. When C_α=75%, the WTS only decreases by 3.2% in comparison with the unstented case (Fig. 7).

4 Conclusions

1. The computed stented intra-aneurysmal flow pattern is found to be in good accord with the experimental one.
2. In general the number and size of structured vortices which featured the streamwise intra-aneurysmal main flow pattern are reduced after stenting. The rotational directions, velocity magnitudes, and prevailing zone of the Dean vortices in the cross-sectional plane are reversed, reduced, and gradually confined to the parent vessel, respectively, after stenting.
3. The average inflow velocity over one cardiac cycle at the aneurysmal neck and fundus decrease exponentially, i.e. $e^{-0.022C_\alpha}$ and $e^{-0.048C_\alpha}$, respectively, with increasing blocking ratio.
4. The wall shear rate of the dome region decrease following the $e^{-0.05C_\alpha}$ distribution as the blocking ratio increases.

References:

[1] Sahs, A.L., Observations on the Pathology of Saccular Aneurysms, *Journal of Neurosurg*, Vol.24, 1966, pp. 79-806.

[2] Suzuki, J., Ohara, H., Clinicopathological Study of Cerebral Aneurysm: Origin, Rupture, and Growth, *Journal of Neurology*, Vol.20, 1978, pp. 74-78.

[3] Crawford, T., Some Observations of the Pathogenesis and Natural History of Intracanical Aneurysm, *Journal of Neurology Neurosurg Psychiatry*, Vol.22, 1959, pp. 259-266.

[4] Dotter, C.T., Judkins, M.P., Transluminal Treatment of Arteriosclerotic Obstruction: Description of a New Technique and a Preliminary Report of Its Application, *Circulation*, Vol.30, 1964, pp.654–670.

[5] Wakhloo, A.K., Schellhammer, F., Vries, J.D., Haberstroh, J., Schumacher, M., Self-Expanding and Balloon-Expandable Stents in The Treatment of Carotid Aneurysms: An Experimental Study In a Canine Model, *American Journal of Neuro-radiology*, Vol.15, 1994, pp. 493–502.

[6] Liepsch, D.W., Steiger, H.J., Poll, A., Reulen, H.J., Hemodynamic Stress In Lateral Saccular Aneurysms, *Biorheology*, Vol.24, 1987, pp. 689-710.

[7] Liou, T.M., Liao, C.C., Flowfields In Lateral Aneurysm Arising From Parent Vessels with Different Curvatures Using PTV, *Experiments in Fluids*, Vol.23, 1997, pp. 288-298.

[8] Liou, T.M., Liou, S.N., Pulstile Flows In a Lateral Aneurysm Anchored on a Stented and Curved Parent Vessel, *Journal of Experimental Mechanics*, Vol.44, 2004, pp.253-260.

[9] Burleson, A.C., Strother, C.M. Turitto, V.T., Computer Modeling of Intracranial Saccular and Lateral Aneurysms for the Study of Their Hemodynamics, *Neurosurgery*, Vol.37, 1995, pp. 774-784.

[10] Löw, M., Perktold, K., Rauning, R., Hemodynamics In Rigid and Distensible Saccular Aneurysms: A Numerical Study of Pulsatile Flow Characteristics, *Biorheology*, Vol.30, 1993, pp. 287-298.

[11] Liou, T.M., Li, Y.C., Juan, W.C., Numerical and Experimental Studies on Pulsatile Flow Inside Lateral Aneurysms Arising From a Curved Parent Vessel at Various Angles, *Journal of Bio-mechanics* (In Press)

[12] Stuhne, G.R., Steinman, D.A., Finite Element Modeling of the Hemodynamics of Stented

Aneurysms, *Journal of Biomechanical Engineering*, Vol.126, 2004, pp. 382-387.

[13] Bando, K, Berger, S.A., Research on Fluid Dynamic Treatment of Aneurysms by Means of Computational Simulation, *Computational Fluid Dynamics J*ournal, Vol. 11, 2003, pp. 527-531.

[14] Nagasawa, S., Kawanishi, M., Tada, Y., Kawabata, S., Ohta, T.,X Intra-Operative Measurement of Cortical Arterial Flow Volumes in Posterior Circulation Using Doppler Sonography, *Neurological research*, Vol.22, 2003, pp. 194-196.

[15] Zhang, Y.Z., Zhang, X.L., Chang, R.M., Cang, P., Liou, X.Y., Xia, Q., Diameter Measure-Ments of Cerebral Arteries on Three-Dimensional Time-of-Flight MR Angiograms, *Chinese Journal of Radiology*, Vol.37, 2003, pp. 394-398.

[16] Cebral, J.R., Lohner, R., Soto, O., Yim, P.J., On the Modeling of Carotid Artery Blood Flow From Magnetic Resonance Images, *Bio-engineering Conference ASME2001*, Vol.50, 2001, pp. 619-620.

[17] Raithby, G.D., Van Doormaal, J.P., Enhancements of the SIMPLE Method for Predicting Incompressible Fluid Flow, *Numerical Heat Transfer*, Vol.7, 1984, pp. 147-163.

[18] Tominaga, R., Harasaki, H., Sutton, C., Emoto, H., Kambic, H., Hollman, J., Effect of Stent Design and Serum Cholesterol Level on the Restenosis Rate in Atherosclerotic Rabbits, *American Heart Journal*, Vol.126, 1993, pp. 1049-1058.

[19] Moore, J.E., Xu, C., Glagov, S., Zarins, C.K., Ku, D.N., Fluid Wall Shear Stress Measurements in a Model of the Human Abdominal Aorta: Oscillatory Behavior and Relationship to Atherosclerosis, *Atherosclerosis*, Vol.110, 1994, pp. 225-240.

[20] Lieber, B.B., Stancampiano, A.P., Wakhloo, A.K., Alteration of Hemodynamics in Aneurysm Models by Stenting: Influence of Stent Porosity, *Annals of Biomedical Engineering*, Vol.25, 1997, pp. 460-469.

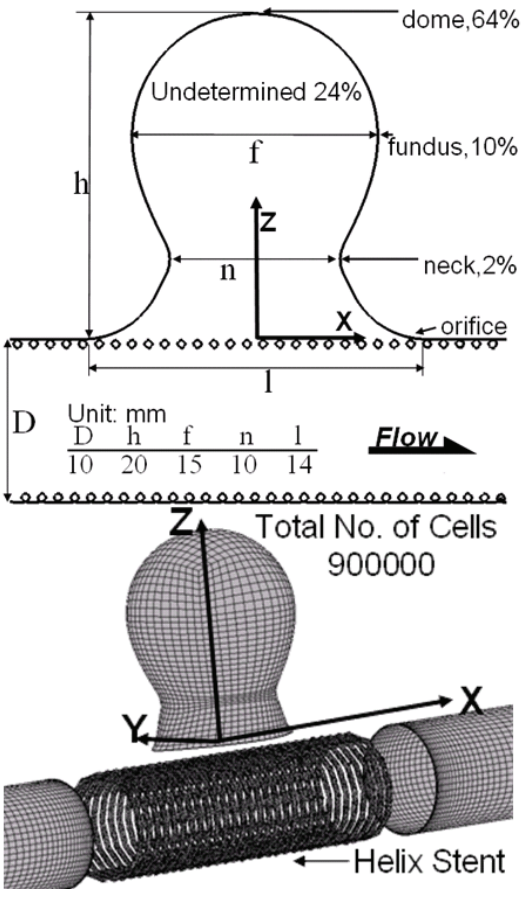

Fig. 1 Configuration, Coordinate system, dimensions, and grid distribution of main computational domain (Percentage denotes fraction of local ruptures (Crawford, 1959))

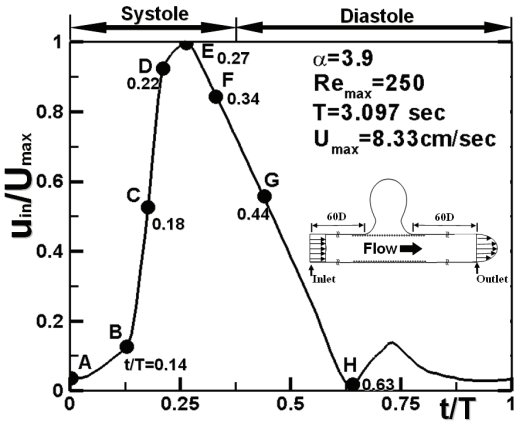

Fig. 2 Time-resolved velocity waveform at 60D upstream of aneurysmal pore of PCA (Cebral et al., 2001)

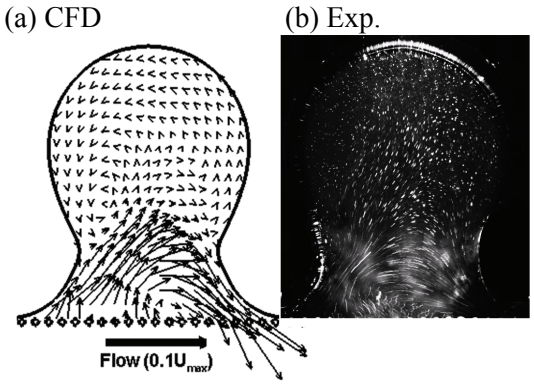

Fig. 3 Stented intra-aneurysmal main flow patterns at t/T=0.34 phase (Re=210) of Fig.2 for C_α=50% (a) CFD (b) Exp.

(a) C_α=0%

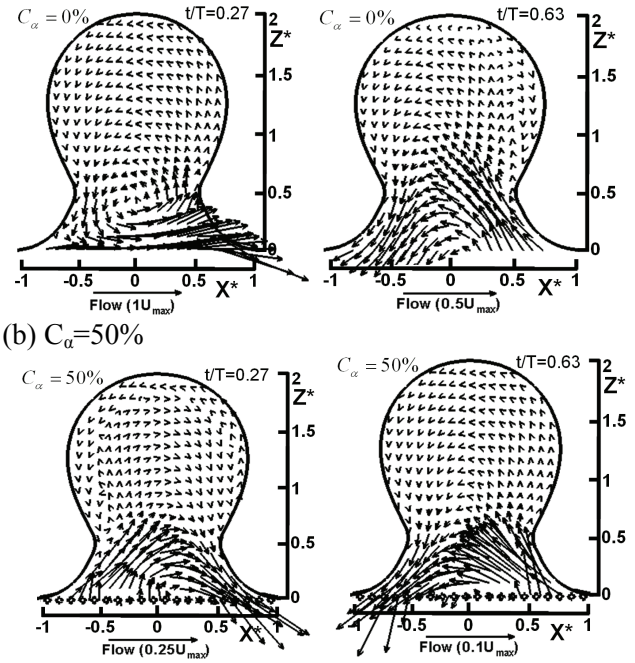

Fig. 4 Computed intra-aneurysmal velocity vector fields in Y*=0 plane at some selected flow rate phases for (a)unstented and (b)stented cases (Re_{max}=250, α=3.9)

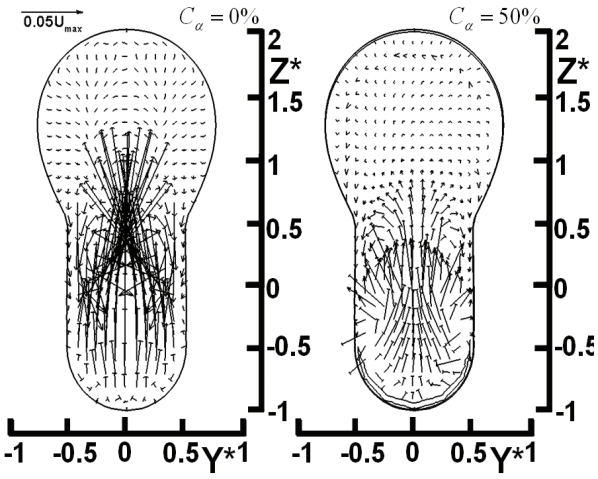

Fig. 5 Secondary flow patterns in X*=0 plane in terms of velocity vector fields at peak flow rate phase for unstented and stented cases (Re_{max}=250, α=3.9, t/T=0.27; the parent flow is pointed out of paper plane)

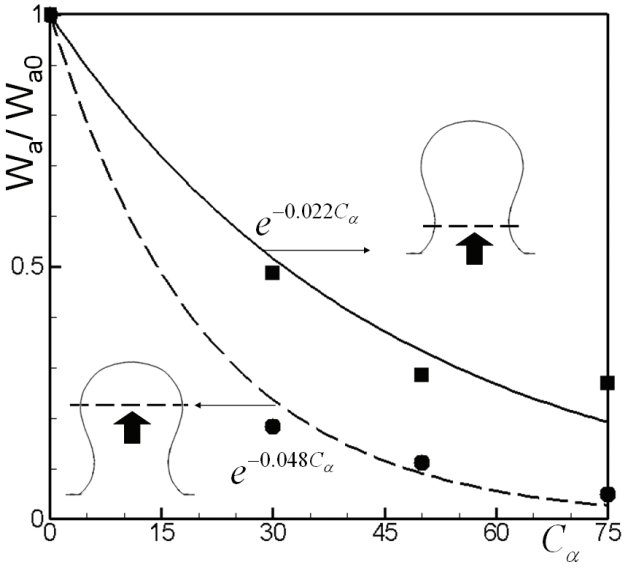

Fig. 6 Average inflow velocity at the neck and the fundus over one cardiac cycle as a function of C_α when the values for unstented aneurysm are used as a baseline

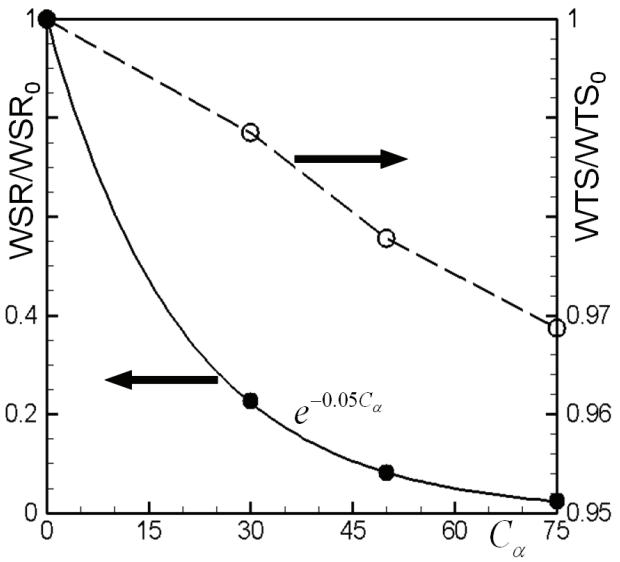

Fig. 7 Variation of wall shear rate and wall pressure at dome region with blocking ratio